Solar Energy Materials and Solar Cells 173 (2017) 43–49

Contents lists available at ScienceDirect

Solar Energy Materials and Solar Cells

journal homepage: www.elsevier.com/locate/solmat

Increasing the efficiency of silicon heterojunction solar cells and modules by light soaking

Eiji Kobayashi[a,b,c,*], Stefaan De Wolf[d], Jacques Levrat[e], Antoine Descoeudres[e], Matthieu Despeisse[e], Franz-Josef Haug[a], Christophe Ballif[a,e]

[a] École Polytechnique Fédérale de Lausanne (EPFL), Institute of Microengineering (IMT), Photovoltaics and Thin Film Electronics Laboratory, Rue de la Maladière 71b, CH-2002 Neuchâtel, Switzerland
[b] Choshu Industry Co., Ltd., 3740, Shin-yamanoi, Sanyo Onoda, Yamaguchi 757-8511, Japan
[c] Department of Materials Science and Engineering, Yamaguchi University, 2-16-1 Tokiwadai, Ube, Yamaguchi 755-8611, Japan
[d] King Abdullah University of Science and Technology (KAUST), KAUST Solar Center (KSC), Thuwal 23955-6900, Saudi Arabia
[e] CSEM PV-Center, Jaquet-Droz 1, CH-2002 Neuchâtel, Switzerland

ARTICLE INFO

Keywords:
Solar cell
Solar module
Silicon heterojunction
Passivating contact
Light soaking
Fill factor

ABSTRACT

Silicon heterojunction solar cells use crystalline silicon (*c*-Si) wafers as optical absorbers and employ bilayers of doped/intrinsic hydrogenated amorphous silicon (*a*-Si:H) to form passivating contacts. Recently, we demonstrated that such solar cells increase their operating voltages and thus their conversion efficiencies during light exposure. We found that this performance increase is due to improved passivation of the *a*-Si:H/*c*-Si interface and is induced by injected charge carriers (either by light soaking or forward-voltage biasing of the device). Here, we discuss this counterintuitive behavior and establish that: (i) the performance increase is observed in solar cells as well as modules; (ii) this phenomenon requires the presence of *doped* *a*-Si:H films, but is independent from whether light is incident from the *a*-Si:H(*p*) or the *a*-Si:H(*n*) side; (iii) UV and blue photons do not play a role in this effect; (iv) the performance increase can be observed under illumination intensities as low as 20 W m^{-1} (0.02-sun) and appears to be almost identical in strength when under 1-sun (1000 W m^{-1}); (v) the underlying physical mechanism likely differs from annealing-induced surface passivation.

1. Introduction

Silicon wafers with excellent bulk electronic properties and layers providing high-quality surface passivation are now widely available for realizing solar cells. Consequently, carrier recombination at the electrical contacts is now the major electronic loss in silicon solar cells, because direct metal/silicon interfaces feature a high density of recombination-active localized states. This high surface-state density increases the recombination rate of photo-generated or injected carriers at the interface. Such recombination can be mitigated by introducing a high surface doping which screens the metal/silicon contacts from minority carriers. The so-called passivating-contact technologies aim at minimizing these losses by drastically reducing the surface-state density of silicon near the contact. To this end, films made from intrinsic hydrogenated amorphous silicon (*a*-Si:H) are a particularly attractive choice for solar cells because they are at the same time conductive (if thin enough) and they provide excellent passivation of crystalline silicon (*c*-Si) surfaces by removing the *c*-Si surface states, even when they are only a few nanometers thick [1–5]. Moreover, such films can be doped, increasing further their functionality [6]. When effectively doped, *a*-Si:H films usually do not exhibit good passivation, but when they overlay thin intrinsic *a*-Si:H layers, they can efficiently collect either electrons or holes (in case of *n*-type and *p*-type overlayers, respectively), while maintaining very high internal voltages [7–10]. Solar cells that feature such doped/intrinsic *a*-Si:H contacts are usually referred to as silicon heterojunction (SHJ) solar cells, which is a technology pioneered by Panasonic, Japan (then Sanyo) [11]. Kaneka, Japan recently demonstrated the effectiveness of SHJ by setting a new single-junction silicon solar cell efficiency record at 26.6% using doped/intrinsic *a*-Si:H contacts in a fully back-contacted layout [12]. In their most simple implementation, SHJ solar cells have electron- and hole-collecting contacts on the opposite sides of the wafer. The best reported efficiency for this implementation is 25.1%, also established by the same company [13].

Long-term stability under actual operating conditions is an important criterion for any solar technology. In this context, conflicting

* Corresponding author at: École Polytechnique Fédérale de Lausanne (EPFL), Institute of Microengineering (IMT), Photovoltaics and Thin Film Electronics Laboratory, Rue de la Maladière 71b, CH-2002 Neuchâtel, Switzerland.
E-mail address: kobayashi.eiji@choshu.co.jp (E. Kobayashi).

http://dx.doi.org/10.1016/j.solmat.2017.06.023
Received 28 March 2017; Received in revised form 31 May 2017; Accepted 16 June 2017
Available online 24 June 2017

data on the stability of SHJ-based photovoltaics have been reported. For example, Jordan *et al.* reported that SHJ modules degrade at a faster rate than do other *c*-Si based modules (1% versus 0.5–0.8% annual degradation, respectively) [14]. However, Sharma et al. found an increase in V_{oc} of a SHJ module after 28 months in the field [15]. Recently, we demonstrated that light soaking (LS) of SHJ solar cells increases their open circuit voltage (V_{oc}) and fill factor (*FF*), leading to a gain in absolute conversion efficiency of up to 0.3% [16]. In particular, we found that the electronic passivation of *c*-Si surfaces coated with *p*- or *n*-type doped *a*-Si:H films or with bilayers of *p*- or *n*-type/intrinsic *a*-Si:H under prolonged LS was improved. Mahtani *et al.* reported a similar trend for *p*-type/intrinsic *a*-Si:H bilayers [17]. Based on these results, the loss in SHJ module performance reported by Jordan et al. may not have been the result of light-induced cell degradation, but arguably was caused by other factors, possibly linked to early-generation technology. Despite its direct beneficial impact on power generation of SHJ-based photovoltaics, light-induced performance improvement is not yet well understood. However, fundamental insight into the underlying physics of light-induced performance may lead to further device sophistication, increasing performance. Performance improvement under LS is actually unusual, as most silicon-based technologies are either stable or exhibit degradation under LS conditions. A classic example of light-induced degradation (LID) is the so-called Staebler–Wronski effect (SWE), which degrades the performance of thin-film *a*-Si:H solar cells [18–21]. Another example of LID is associated with *p*-type, *c*-Si-based solar cells, caused by the formation of a recombination-active boron-oxygen complex in the bulk of the wafer [22,23]. In contrast, V_{oc} improvement induced by light soaking is well known in both major thin-film technologies CdTe [24] and CIGS [25]. In addition, V_{oc} improvement induced by light soaking has been reported for *a*-Si:H devices by a variety of institutes and explained [26].

Perhaps counterintuitively, it is possible that light-induced performance improvement in SHJ cells is related to SWE. In this case, remarkable *FF* improvement is also observed as well as V_{oc} improvement. Previously, we found that the passivation of *intrinsic* *a*-Si:H/*c*-Si interfaces decays upon long-term LS, following identical kinetics (in the form of power laws) to that for LID in bulk *a*-Si:H solar cells [27]. The underlying kinetics of *doped* *a*-Si:H/*c*-Si interfaces is also similar to that of SWE, as indicated by power laws [16]. Recently, Melskens *et al.* discussed the degradation mechanism of SWE, but its kinetics can impossibly be described by single time scaling ($\sim t^{\beta}$), which means that some parts remain unexplained [28]. The effect of doping, and more generally the position of the Fermi-level, in bulk *a*-Si:H is described in defect-pool models [29–35], but the effect of LS on such doped layers on a *c*-Si absorber remains unclear, doubtlessly because thin-film *a*-Si:H devices are exclusively fabricated in a so-called *p-i-n* configuration, with the optically active absorber consisting of intrinsic *a*-Si:H [36], where the Fermi-level never deviates much from midgap.

Similarities and differences between earlier findings around LS raise several important questions about the precise impact of the *a*-Si:H/*c*-Si heterointerface. For example, in *a*-Si:H/nanocrystaline (*nc*)-Si double junction solar cells, LID is mainly observed in the top cell, because the *a*-Si:H top cell absorb most of the high-energy photons [37]. Additionally, low-energy photons just above the bandgap of *a*-Si:H still lead to a degradation of the top cell. How do the high-energy photons play a role in the LS effect? Moreover, the degree of SWE in bulk *a*-Si:H is related to the carrier recombination rate which is related to the generation rate G_e, and thus to the applied light intensity [38]. Does the LS effect similarly depend on light intensity? Finally, post-deposition passivation improvement by low-temperature annealing (< 200 °C) is a well-known phenomenon in SHJ solar cells [39]. To what extent does its underlying mechanism hold relevance to the light-induced improvement of SHJ cells? Related to this, will post-annealing after LS improve SHJ solar cells? Here, we seek answers to these questions by describing the LS phenomenon in SHJ solar cells in detail.

2. Experimental details

To evaluate current density–voltage (*J–V*) characteristics under LS, we fabricated four types of SHJ solar cells and a precursor. Two of the four types were 3-busbar solar cells, one with front-emitter (sample set A) and the other with rear-emitter (sample set B). Both 3-busbar types were 243.4 cm^2 in size. The other two of the four types were busbarless solar cells, one with rear-emitter (sample set C) and the other with front-emitter (sample set D). Sample set C were 243.4 cm^2 in size. Sample set D were a 4 cm^2 device with contact electrodes for 4-point probes method to evaluate *J–V* characteristics under LS at selected wavelengths. We also fabricated solar cell precursors, missing transparent conductive oxide (TCO) layers and electrodes (sample set E), for evaluating minority carrier lifetimes under LS with different light intensities. We used *n*-type Czochralski Si(100) wafers (with a resistivity of 2.9 Ω cm) as absorbers in all four SHJ solar cell designs and a precursor of finished cells. These wafers were textured in an alkaline solution and wet-chemically cleaned. The textured wafers (with a thickness of 180 μm) were then dipped in 5% hydrogen fluoride solution just before plasma-enhanced chemical vapor deposition (PECVD). The intrinsic (*i*) and doped (*n* and *p*) *a*-Si:H layers were deposited on both wafer surfaces at 200 °C using mixtures of SiH_4, PH_3, $B(CH_3)_3$, and H_2 in a PECVD tool operated at 13.56 MHz. Schematics of the fabricated cells and precursors are shown in Fig. 1. Our analysis focuses on the asymmetric *i-p/i-n* solar cell precursor; we used 6-nm-thick *i* layers for finished cell structures and test structures. The *n* and *p* layers of the finished cell structures were 3-nm thick and these layers of the test structures were 6-nm thick (see Fig. 1). Thicknesses for each *a*-Si:H layer were measured on textured surfaces and calculated from the angle of the texture as visualized by a cross-sectional transmission electron microscope. On the finished cells, indium tin oxide (ITO) films were sputter-deposited as TCO layers on both sides of the wafer, which were then capped with a silver reflector, which was also sputter-deposited, at the rear. Front electrodes (fingers and busbars) were screen-printed from a low-temperature silver paste on the front ITO layer. Finally, the cells were cured at 200 °C for 30 min.

Before LS, pre-annealing was conducted at 200 °C in air under dark conditions. LS was then carried out in a commercial system (Sunirad A-65, Solaronix) under Air Mass 1.5 global (AM 1.5G) illumination (CLASS A, International Electrotechnical Commission (IEC) 60904-9/American Society for Testing and Materials (ASTM) E927-05). The substrate temperature was maintained during LS at 32 ± 2 °C by a water-cooling system, to eliminate a possible temperature induced improvement [40]. To track electronic changes at the *a*-Si:H/*c*-Si heterointerface, excess carrier lifetimes, τ_{eff}, of the wafers were measured with the transient photoconductance technique (WCT-120, Sinton Instruments), which complied with Semiconductor Equipment and Materials International (SEMI) standard PV-13 [41]. The stage temperature during the τ_{eff} measurements was 24 ± 1 °C. The finished SHJ cells were characterized by current–voltage measurements on a 1-sun solar simulator under 1000 W m^{-2} AM 1.5G illumination at 25 ± 0.1 °C by a water-cooling system. To estimate the measurement error, we carried out the cross-check measurements between our site and Japan Electrical Safety and Environment Technology Laboratories (JET) using SHJ solar cells (sample set B, five cells). Consequently, the measurement error was expected to be less than ± 0.1% absolute to cell efficiencies. The external quantum efficiency (EQE) was measured with a spectral response measurement system (CEP-25RR, Bunkokeiki).

3. Results and discusion

Fig. 2 illustrates changes in the conversion efficiency (η) of finished SHJ solar cells using LS under open-circuit conditions with two different light incident directions, one from the *a*-Si:H(*p*) side, the other from the a-Si:H(*n*) side (sample set A and B, respectively, see also Fig. 1). In this graph, $t_{1\text{-}sun}$ is the 1-sun LS time. The averaged initial

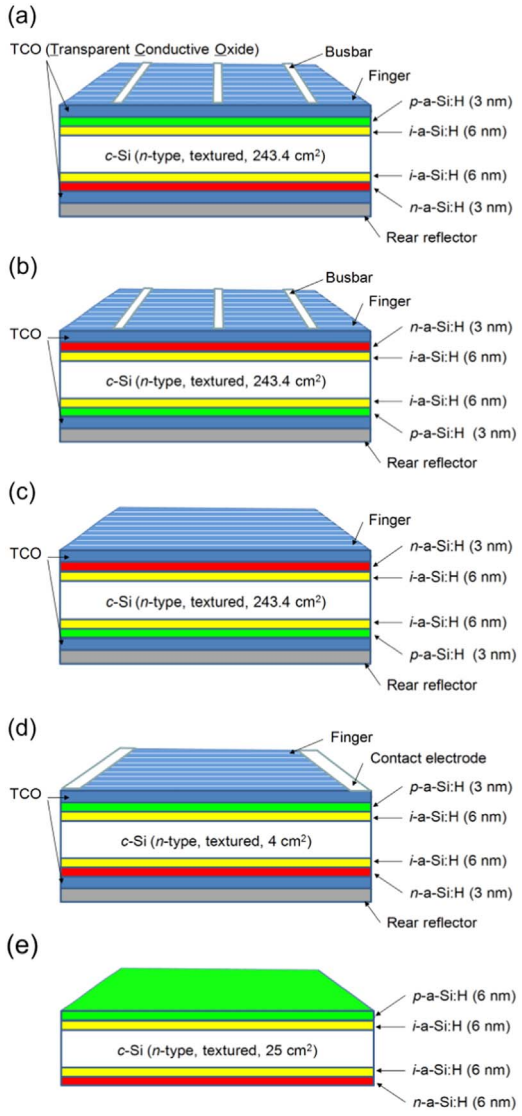

Fig. 1. Schematic of the four silicon heterojunction solar cell structures and a precursor (not to scale). (a) Sample set A: 3-busbar cell with front-emitter. (b) Sample set B: 3-busbar cell with rear-emitter. (c) Sample set C: Busbarless cell with rear-emitter. (d) Sample set D: Busbarless cell with front-emitter. (E) Sample set E: Precursor of finished cells without TCO layers and electrodes.

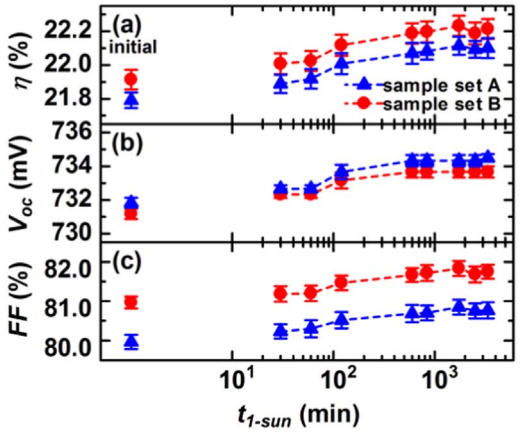

Fig. 2. Measured η values of SHJ solar cells. The values represent averaged characteristics. Each error bar represents the standard error. (a)–(c) Effects of prolonged light exposure as a function of $t_{1\text{-}sun}$. For sample set A, light is incident from the *a*-Si:H (*p*) side; for sample set B, light is incident from the *a*-Si:H (*n*) side. Total cell numbers of each structure are six.

values of η of sample set A and sample set B were 21.8% and 21.9%, respectively. A very similar absolute gain of about 0.3% was observed during LS in both configurations, mainly driven by increasing V_{oc} and *FF* values. It is well established that UV and blue photons can be parasitically absorbed at the front of SHJ devices [42]. However, the identical behavior we observe here in both cases (hole or electron contact at the front) suggests that the performance improvement cannot be caused by absorption of such photons in the front-contacting stacks. This result suggests that light-induced performance gains are obtained in any type of SHJ-based device. An identical cell efficiency gain was observed under forward-voltage bias at 2.8 V and 41 mA cm^{-2} in the absence of illumination [16], indicating that the performance increase in SHJ cells is driven by carrier injection. Classically, in a solar cell, photogenerated carriers either contribute to device current, else they recombine. However, we found earlier that LS also leads to carrier lifetime improvements, as shown in contactless lifetime measurements. This suggests that injected carriers recombine to cause the passivation improvement, and it may well be speculated that the liberated energy from such recombination may aid in nearby interface-state healing. In addition, although we increased the forward-current up to 82 mA cm^{-2} (20A for a single cell, using the mentioned carrier-injected samples after performance increase) in the absence of illumination, no onset of performance degradation was observed (data shown in Supplementary material). We then focused on the solar module structure with an encapsulation material acted as a UV absorber; using sample set C, two Smart Wire Connection Technology (SWCT) modules (C-1 and C-2 in Table 1) featuring a single cell were produced. Details on SWCT can be found in Ref. [43]. A similar efficiency gain in the range of 0.3–0.4% is observed in SWCT single-cell modules after prolonged LS with 1-sun for 330 h (two weeks) under open-circuit conditions (parameters in Table 1). Hence, the modules made out of SHJ solar cells show a 0.3% absolute gain following light exposure. The magnitude of the efficiency gain was slightly changed, mainly due to slight differences in *FF* gain, which may originate from the extrinsic recombination centers (observed as dark areas in electroluminescence images, data shown in Supplementary material) caused by scratched damages in wafer handling systems and wafer cassettes for the manufacturing. Certainly, the dark area (especially seen at the edge) of C-2 with 0.3% gain was wider than C-1 with 0.4% gain. This result suggests that there is a possibility to obtain over 0.3% efficiency gain when we can remove such scratch-induced areas.

To study the role of the illumination spectrum further, we used six types of long-pass glass filters with sharp spectral cut-offs (GG395, GG495, OG590, OG695, RG830, and RG1000, Schott AG) to illuminate the solar cells with photons of selected energy levels. The size of the glass filters was 25 cm^2 (5 cm × 5 cm). Fig. 3a and b respectively show the measured values of the transmittance spectra of the filters and the EQE in SHJ solar cells (sample set D) as measured on each glass filter, respectively. In this graph, λ and λ_c are the wavelength and the cut-off wavelength. In Fig. 3b, the dashed line shows the measured EQE under short-circuit conditions without glass filters. Calculated current densities were obtained from the spectral overlap between the AM 1.5G (1000 W m^{-2}) spectrum and the EQE spectra of the cells with and without long-pass filters. Without λ_c and with λ_c of 395 nm, 495 nm,

Table 1
Single cell module parameters of short-circuit current density (J_{sc}), V_{oc}, *FF*, and η before and after prolonged light soaking. The modules consist of Smart Wire Connection Technology based on silicon heterojunction basbarless solar cells (sample set C). Both single cell modules (C-1 and C-2) were fabricated at the same batch processing.

Sample ID	Light soaking	J_{sc} (mA cm^{-2})	V_{oc} (mV)	*FF* (%)	η (%)
C-1	Before	36.5	731	77.8	20.8
	330 h	36.5	734	79.2	21.2
C-2	Before	36.6	734	77.8	20.9
	330 h	36.6	736	78.5	21.2

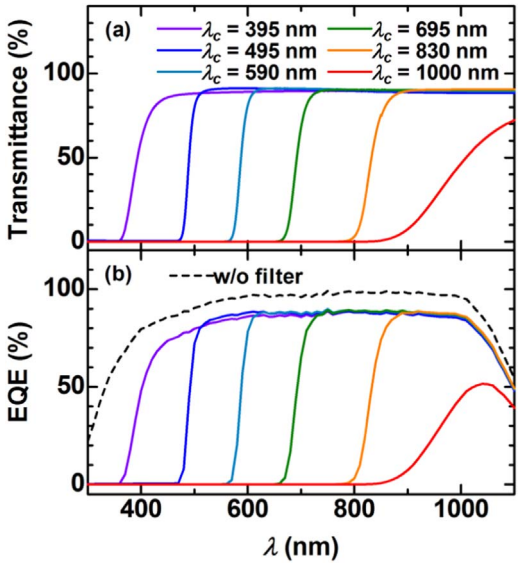

Fig. 3. Measured optical properties of (a) optical long-pass filters and (b) corresponding EQE of SHJ solar cells (sample set D) measured with the long-pass filters.

590 nm, 695 nm, 830 nm, and 1000 nm, the corresponding short circuit densities are 40.0 mA cm^{-2}, 35.1 mA cm^{-2}, 32.0 mA cm^{-2}, 26.7 mA cm^{-2}, 20.1 mA cm^{-2}, 12.1 mA cm^{-2}, and 4.23 mA cm^{-2}, respectively.

Fig. 4 shows the normalized output characteristics of SHJ solar cells (sample set D) after LS under 1-sun for 14 h, during which the efficiency reached saturation. For these experiments, nine cells were made per wafer and they were defined by the area of the front transparent electrode, which was made from ITO. It is evident from the data that unexpectedly identical η gains were obtained for any photon exposure between the UV and near-infrared regions using identical light-exposure times, suggesting that the LS effect cannot be attributed to UV and blue photons that are absorbed by the *a*-Si:H layers. Indeed, with a typical bandgap of about 1.7 eV, light with wavelengths longer than about 700 nm cannot be absorbed directly by *a*-Si:H layers. However,

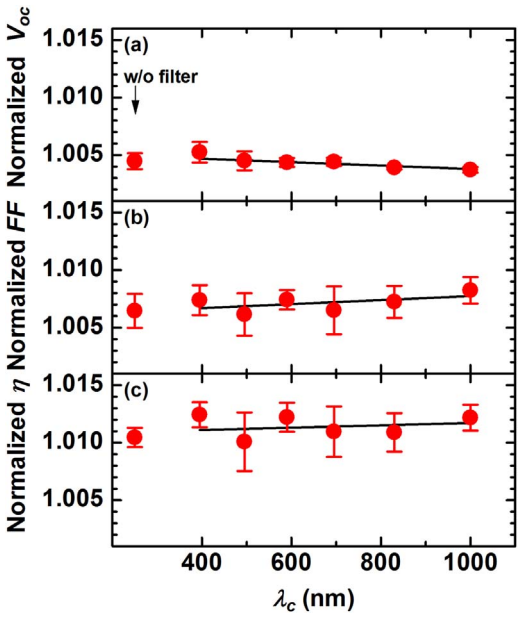

Fig. 4. Measured η values of SHJ solar cells (sample set D) before and after LS for 14 h without and with the long-pass filters shown in Fig. 3, plotted as function of λ_c. The values represent averaged characteristics. Each value is normalized to its corresponding initial η value. Each error bar represents the standard error. Total cell numbers are six at each point. Solid lines are the linear least-square fits.

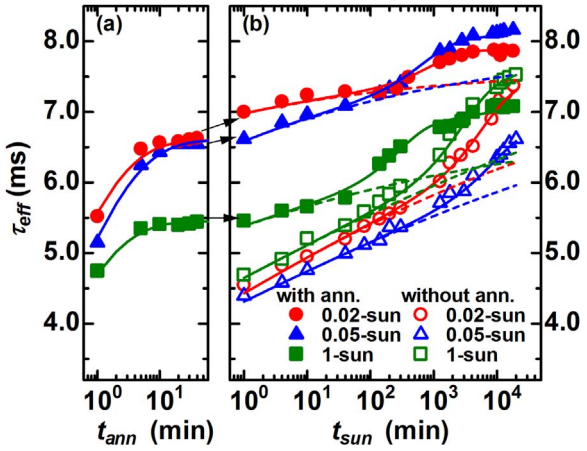

Fig. 5. Changes in the minority carrier lifetime during a repeated cycle of (a) 200 °C annealing and (b) LS with 0.02-, 0.05-, and 1-sun with sample set E. The light is incident from the *p*-*a*-Si:H side. The evaluation was performed at the injection of 1 × 10^{15} cm^{-3}. Symbols indicate measured data. (a)Solid lines show stretched exponential fits [40]. (b) Solid lines show power law and field effect fits [16]. Dashed lines show only the power law part. Values for coefficient of determination (R^2) are 0.99 in all fits. Values for each fitting parameters are given in Table 2.

our results clearly suggest that the performance improvement is also driven by light that has a wavelength *longer* than the 1000 nm cut-off filter, implying that it must be caused by carriers injected into the *c*-Si, which then 'aid' defect healing at the *a*-Si:H/*c*-Si interface. We note that, for example, the calculated light intensity of the near infrared region (λ_c = 1000 nm) corresponds to only 0.1-sun, although an identical η gain was observed using only this reduced part of the spectrum.

We analyzed the interfaces in our devices that were exposed to different light intensities. In the same experiments, we verified the impact of pre-annealing the films. To decrease the light intensity, we used a neutral-density (ND) glass filter with a flat transmission profile for wavelengths greater than 300 nm (data shown in Supplementary material) and then adjusted the light intensity of the system. Again, the size of the glass filters was 25 cm^2 (5 cm × 5 cm). The light intensity was calibrated by a reference cell that complied with the IEC60904-2 standard for *c*-Si solar cells.

Fig. 5 shows how *a*-Si:H/*c*-Si interface passivation evolves over repeated pre-annealing/LS cycles in an *i*-*p*/*i*-*n* solar cell precursor (sample set E), where t_{sun} and t_{ann} is the LS time and annealing time, respectively. We prepared six precursors for this experiment, three of which underwent the pre-annealing treatment at 200 °C in the dark. The pre-annealing treatment was applied until τ_{eff} saturation was reached. The LS treatment was then carried out on all precursors at three light intensities: 0.02-, 0.05-, and 1-Sun. In classic SWE in bulk *a*-Si:H, the degradation is known to scale directly with the generation rate. Here, τ_{eff} increased during LS, but we did not observe an influence of the light intensity on the extent of the passivation improvement. Although the passivation reached saturation in the pre-annealed samples [44], we found that subsequent LS led to a further increase in τ_{eff}. This suggests that improvements from pre-annealing and LS have fundamentally different sources as discussed below.

Previously, isothermal-annealing was found to induce changes in the surface passivation of intrinsic *a*-Si:H/*c*-Si interfaces [39]. Fig. 5a shows that our experimental annealing data – before LS – agree with the calculated fits (fitting parameters shown in Table 2) [40]. Quite generally, stretched exponentials are often associated with the relaxation of disordered systems over time towards equilibrium [45,46]. For bulk *a*-Si:H, relaxation has been argued to be governed by the release of hydrogen from the trap sites that then reduces the density of recombination-active interface states (e.g., Si dangling bonds), leading to electronically improved material [47]. In our devices, the annealing-

Table 2
Parameters of stretched exponential (SE) fits in Fig. 5a and power law (PL) fits in Fig. 5b. The formulae of SE and PL forms are presented in Ref. [40] and [16], respectively. τ_{eff}^{SS} is the saturation value for τ_{eff}, τ_0 and τ_1 are effective time constants, β is the dispersion parameter ($0 < \beta < 1$), a_1 is a constant.

	Model	τ_{eff}^{SS} (ms)	τ_0 (min)	β	a_1 (ms)	τ_1 (min)
Ann, for 0.02-sun	SE	6.60	0.17	0.35		
Ann, for 0.05-sun	SE	6.60	0.28	0.35		
Ann, for 1-sun	SE	5.45	0.14	0.35		
0.02-sun w/o ann	PL	7.70	8×10^{-2}	0.12	1.05	6000
0.02-sun w/ ann	PL	7.60	1×10^{-7}	0.15	0.45	900
0.05-sun w/o ann	PL	7.70	9×10^{-2}	0.10	0.70	9000
0.05-sun w/ ann	PL	7.90	1×10^{-5}	0.14	0.60	700
1-sun w/o ann	PL	8.30	9×10^{-2}	0.10	1.10	3000
1-sun w/ ann	PL	6.90	1×10^{-5}	0.11	0.75	300

induced improvement reached saturation after 20 min. Earlier, we found by Fourier-transform infrared (FTIR) spectroscopy that changes in passivation by annealing at the intrinsic *a*-Si:H/*c*-Si interface are actually driven by changes in the microstructural Si-H bonding environment. Accordingly, the onset of passivation saturation was observed to occur as soon as microstructural changes ceased to be observable [40]. We also found that LS does not lead to FTIR-observable changes in the microstructure [40]. As indicated in Fig. 5, the 'annealing-saturated' τ_{eff} values further increase during subsequent LS (see panel b). This suggests that the underlying physics of light induced passivation is different from that which is annealing induced. The results shown in Fig. 5 are for solar cell precursors. Actual SHJ solar cells, such as those presented Figs. 2 and 4, normally include a 200 °C annealing process to cure the printed silver electrode. The τ_{eff} increase in pre-annealed cells is therefore consistent with the results in Figs. 2 and 4.

In our earlier work [27,40], we found that the decay of intrinsic *a*-Si:H/*c*-Si interface passivation under prolonged illumination follows a modified power-law [16]. The data in Fig. 5b show that eq. 3 in Ref. [16] fits the experimental LS data well (fitting parameters shown in Table 2). The τ_{eff} of pre-annealed cells saturates faster than that of non-annealed cells, perhaps because the pre-annealed cells started LS with a reduced density of interface states. We investigated the repeatability of this time dependence with several cells, all of which followed identical trends.

Fig. 6 shows τ_{eff} curves as a function of the carrier injection level, Δn, during LS (at 1 min and 9960 min) of the pre-annealed *i-p/i-n*

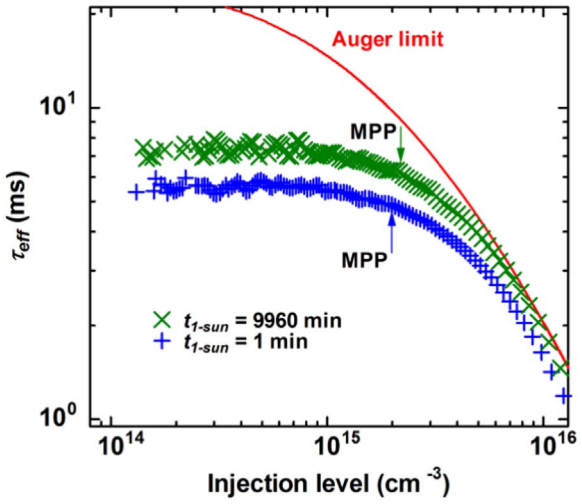

Fig. 6. Measured values for τ_{eff} as a function of the carrier injection level of pre-annealed solar precursors during LS with sample set E. Symbols indicate the measured data. The injection levels corresponding to the maximum power points (MPPs) are marked by solid arrows. Auger recombination limits are shown by the solid line [48].

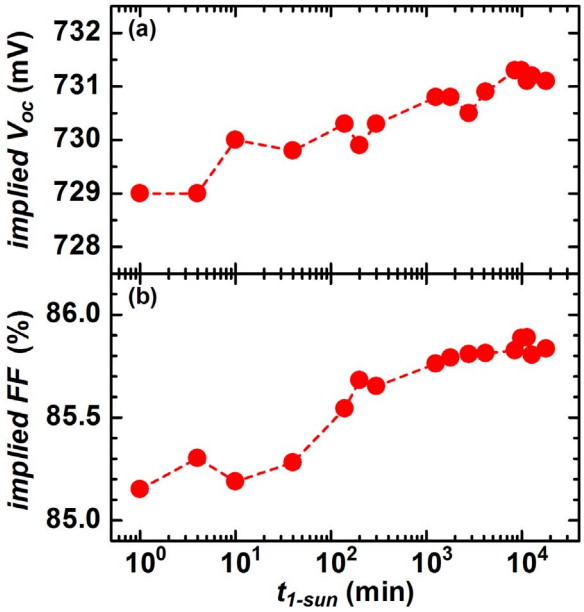

Fig. 7. Calculated (a) *implied* V_{oc} and (b) *implied FF* as functions of $t_{1\text{-}sun}$ from the τ_{eff} of the pre-annealed cell in Fig. 5b.

structure in Fig. 5b. The uppermost solid curve represents the maximum possible bulk lifetime based on the Auger recombination parameterization by Richter et al. [48]. We note that the τ_{eff} values over most of the range of carrier injection level increase markedly during LS. At the higher injection level (around 10^{16} cm^{-3}), the τ_{eff} values exhibit less improvement, but this is because the unavoidable Auger recombination limit dominates at high injection. We quantify the effect on the corresponding operating voltages by calculating the "implied V_{oc}" and the "implied *FF*" from the τ_{eff} data collected from a device kept at open circuit [49], which is similar to Suns-V_{oc} measurements [50]. The implied *FF* values exclude series resistance and issues related to transport and extraction of carriers through the contacts. Fig. 7 shows the "implied V_{oc}" and the "implied *FF*" calculated from the τ_{eff} data of a pre-annealed precursor, subsequently exposed to 1-sun LS (see Fig. 5b), leading to an increase of 2.4 mV and 0.72%, respectively, after 9960 min of exposure. These values correspond to the absolute 0.28% gain (0.08% and 0.2% gain, respectively), which is consistent with the performance increase of finished cells shown in Fig. 2. We conclude that the gain in η during LS is primarily due to an increase of implied *FF* and an improved V_{oc} as a result of a reduced density of recombination-active interface states.

Since the *n*-type wafer material is not expected to performance change during LS, we are led to conclude that the changes take place in the amorphous passivation layers on the *n*-type wafer even though it is puzzling that the changes should be beneficial. Normally, LS result results in a degradation of amorphous silicon due to the creation of light-induced defects that follows the recombination of electrons and holes [51]. However, the saturation of light induced defect-creation could only be explained by assuming that defects can also be healed by recombination effects [52]. In order to assess the possibility of light induced healing, we use the numerical simulation tool Advanced Semiconductor Analysis (ASA) software package (version 5.21) [53] to investigate the carrier recombination rate, R_e, in SHJ solar cells during LS. The main parameters of the different layers used for the solar cell simulations are listed in Table 3 (also see ASA input file shown in Supplementary material). The density-of-states distributions of the *a*-Si:H layers are shown in Fig. 8. Fig. 9a shows the calculated band diagram of a SHJ solar cell during 1-sun LS at V_{oc}. Here, E_c, E_v, $E_{F,n}$, and $E_{F,p}$ are the conduction band energy, valence band energy, electron quasi-Fermi level, and hole quasi-Fermi level, respectively. Fig. 9b shows R_e during 0.02-, 0.1-, and 1-sun LS, again at V_{oc}. The R_e values in

Table 3
ASA simulation parameters.

Parameters	*p*/*i*-*a*-Si		*i*/*n*-*a*-Si		*n*-*c*-Si
Thickness (nm)	5	5	5	5	180 μm
Dielectric constant	11.9	11.9	11.9	11.9	11.8
Electron affinity (eV)	3.8	3.8	3.8	3.8	4.05
Band gap (eV)	1.75	1.75	1.75	1.75	1.124
Effective CB DOS ($cm^{-3}\,eV^{-1}$)	2×10^{20}	2×10^{20}	2×10^{20}	2×10^{20}	2.86×10^{19}
Effective VB DOS ($cm^{-3}\,eV^{-1}$)	2×10^{20}	2×10^{20}	2×10^{20}	2×10^{20}	3.10×10^{19}
Electron mobility ($cm^2\,V^{-1}\,s^{-1}$)	10	20	20	10	1300
Hole mobility ($cm^2\,V^{-1}\,s^{-1}$)	1	5	5	1	400
Activation energy (eV)	0.45	–	–	0.15	–
Donor concentration (cm^{-3})	–	–	–	–	1×10^{16}
Band tails and defects					
VB tail slope (meV)	60	45	45	60	–
CB tail slope (meV)	40	30	30	40	–

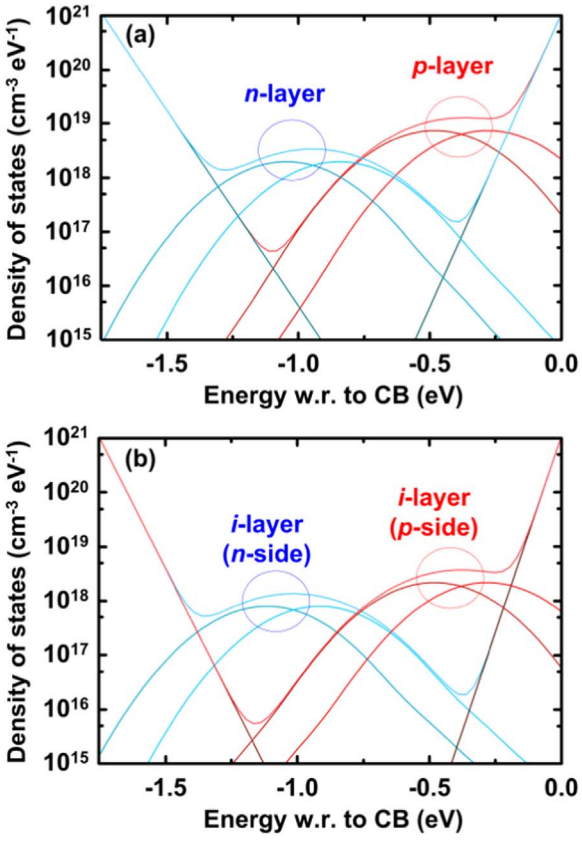

Fig. 8. Simulated defect properties of (a) doped *a*-Si:H and (b) *i*-*a*-Si:H layers.

the *c*-Si absorber close to *a*-Si:H/*c*-Si heterointerface vary over almost three orders of magnitude between 10^{17} and $10^{20}\,cm^{-3}\,s^{-1}$. At the same time, in the amorphous layer that is sandwiched between the wafer and the *p*-doped layer R_e varies only over a much smaller range between 10^{19} and $10^{20}\,cm^{-3}\,s^{-1}$. This means that even low LS-intensities this layer is exposed to recombination rates similar to the case of LS with 1-sun. Concluding that the recombination is fed by a flow of photo-generated carriers from the wafer, the small variation of the actual recombination rate in the layer can explain why the LS effects show no appreciable dependence on the illumination intensity and that they are even observed for illumination with wavelengths that are not absorbed in the amorphous layer.

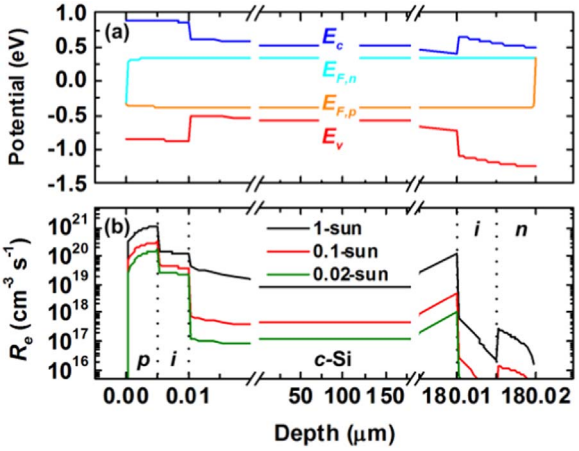

Fig. 9. (a) Band diagram of SHJ solar cells during a 1-sun LS. (b) The carrier recombination rate (R_e) distribution in SHJ solar cells under 0.02-, 0.1-, and 1-sun. The light is incident from the *p*-*a*-Si:H side.

4. Conclusion

In this paper, we clarified several points linked to light-induced performance increase from passivating contacts in *a*-Si:H/*c*-Si heterointerfaces. An increase of τ_{eff} resulted in improved implied V_{oc} and implied *FF* in finished SHJ cells after LS as well as from the application of a dark forward-voltage bias. The performance increase corresponds to a 0.3% absolute gain of η or roughly to a 1.4% relative gain after 150 h under 1-sun. The identical gain of η is also observed in a module structure. The effect is observed when the light is incident on either the side of *p*-*a*-Si:H- or *n*-*a*-Si:H layers. UV and blue photons do not play a role in this effect. The origin of the improvement is a nonradiative recombination process taking place at the interface of photogenerated electron–hole pairs in the *c*-Si absorber. The passivation quality at the *a*-Si:H/*c*-Si heterointerface can be improved under light intensities as low as 20 W m^{-1} (0.02-sun) in a time range similar to the one obtained for 1000 W m^{-1} (1-sun). The time dependence behavior of the τ_{eff} values is described by a modified power law, which contrasts to pre-thermal treatment followed by a stretched exponential form, suggesting that their improvement mechanisms are independent.

Acknowledgements

The authors are grateful to Yoshimi Watabe and Fumiharu Ishimura for the sample preparation of single cell modules. The authors are also grateful to Mathieu Boccard, Gabriel Christmann, Sylvain Nicolay, Philipp Löper, Jan Haschke, Raphaël Monnard, Jean Cattin, Andrea Tomasi, Gizem Nogay, Andrea Ingenito, Philipp Wyss, Josua Stuckelberger, Silvia Martin de Nicolas, Jonathan Champliaud, and Christophe Allebé for fruitful discussions. The simulations were done with the software package ASA of Delft University of Technology. Financial support from the Swiss Federal Office of Energy, EU FP7 program (CHETAAH Project, Contract No. 609788), and King Abdullah University of Science and Technology (KAUST) is acknowledged.

Appendix A. Supporting information

Supplementary data associated with this article can be found in the online version at http://dx.doi.org/10.1016/j.solmat.2017.06.023.

References

[1] H. Fujiwara, M. Kondo, Impact of epitaxial growth at the heterointerface of a-Si:H/c-Si solar cells, Appl. Phys. Lett. 90 (2007) 013503.
[2] S. De Wolf, M. Kondo, Abruptness of a-Si:H/c-Si interface revealed by carrier lifetime measurements, Appl. Phys. Lett. 90 (2007) 042111.

[3] J. Geissbuehler, S. De Wolf, B. Demaurex, J.P. Seif, D.T.L. Alexander, L. Barraud, C. Ballif, Amorphous/crystalline silicon interface defects induced by hydrogen plasma treatments, Appl. Phys. Lett. 102 (2013) 231604.

[4] A. Descoeudres, L. Barraud, S. De Wolf, B. Strahm, D. Lachenal, C. Guérin, Z.C. Holman, F. Zicarelli, B. Demaurex, J. Seif, J. Holovsky, C. Ballif, Improved amorphous/crystalline silicon interface passivation by hydrogen plasma treatment, Appl. Phys. Lett. 99 (2011) 123506.

[5] S. De Wolf, C. Ballif, M. Kondo, Kinetics of a-Si:H bulk defect and a-Si:H/c-Si interface-state reduction, Phys. Rev. B 85 (2012) 113302.

[6] W.E. Spear, P.G. Le Comber, Substitutional doping of amorphous silicon, Solid State Commun. 17 (1975) 1193–1196.

[7] K. Masuko, M. Shigematsu, T. Hashiguchi, D. Fujishima, M. Kai, N. Yoshimura, T. Yamaguchi, Y. Ichihashi, T. Mishima, N. Matsubara, T. Yamanishi, T. Takahama, M. Taguchi, E. Maruyama, S. Okamoto, Achievement of more than 25% conversion efficiency with crystalline silicon heterojunction solar cell, IEEE J. Photovolt. 4 (6) (2014) 1433–1435.

[8] M. Taguchi, A. Yano, S. Tohoda, K. Matsuyama, Y. Nakamura, T. Nishiwaki, K. Fujita, E. Maruyama, 24.7% record efficiency HIT solar cell on thin silicon wafer, IEEE J. Photovolt. 4 (1) (2013) 96–99.

[9] D. Adachi, T. Terashita, T. Uto, J.L. Hernández, K. Yamamoto, Effects of SiOx barrier layer prepared by plasma-enhanced chemical vapor deposition on improvement of long-term reliability and production cost for Cu-plated amorphous Si/crystalline Si heterojunction solar cells, Sol. Energy Mater. Sol. Cells 163 (2017) 204–209.

[10] S. De Wolf, A. Descoeudres, Z.C. Holman, C. Ballif, High-efficiency silicon heterojunction solar cells: a review, Green 2 (2012) 7–24.

[11] M. Tanaka, M. Taguchi, T. Matsuyama, T. Sawada, S. Tsuda, S. Nakano, H. Hanafusa, Y. Kuwano, Development of new a-Si/c-Si heterojunction solar cells: ACJ-HIT (artificially constructed junction-heterojunction with intrinsic thin-layer), Jpn. J. Appl. Phys. 31 (1992) 3518–3522.

[12] K. Yoshikawa, H. Kawasaki, W. Yoshida, T. Irie, K. Konishi, K. Nakan, T. Uto, D. Adachi, M. Kanematsu, H. Uzu, K. Yamamoto, Silicon heterojunction solar cell with interdigitated back contacts for a photoconversion efficiency over 26%, Nat. Energy 2 (2017) 17032.

[13] D. Adachi, J.L. Hernandez, K. Yamamoto, Impact of carrier recombination on fill factor for large area heterojunction crystalline silicon solar cell with 25.1% efficiency, Appl. Phys. Lett. 107 (2015) 233506.

[14] D.C. Jordan, S.R. Kurtz, K. VanSant, J. Newmiller, Compendium of photovoltaic degradation rates, Prog. Photovolt. 24 (2016) 978–989.

[15] V. Sharma, O.S. Sastry, A. Kumar, B. Bora, S.S. Chandel, Degradation analysis of a-Si, (HIT) hetro-junction intrinsic thin layer silicon and m-C-Si solar photovoltaic technologies under outdoor conditions, Energy 72 (2014) 536–546.

[16] E. Kobayashi, S. De Wolf, J. Levrat, G. Christmann, A. Descoeudres, S. Nicolay, M. Despeisse, Y. Watabe, C. Ballif, Light-induced performance increase of silicon heterojunction solar cells, Appl. Phys. Lett. 109 (2016) 153503.

[17] P. Mahtani, R. Varache, B. Jovet, C. Longeaud, J.-P. Kleider, N.P. Kherani, Light induced changes in the amorphous—crystalline silicon heterointerface, J. Appl. Phys. 114 (2013) 124503.

[18] D.L. Staebler, C.R. Wronski, Reversible conductivity changes in discharge-produced amorphous Si, Appl. Phys. Lett. 31 (1977) 292–294.

[19] H.M. Branz, M. Silver, Potential fluctuations due to inhomogeneity in hydrogenated amorphous silicon and the resulting charged dangling-bond defects, Phys. Rev. B 42 (1990) 7420–7428.

[20] D. Redfield, R.H. Bube, Identification of defects in amorphous silicon, Phys. Rev. Lett. 65 (1990) 464–467.

[21] H. Plagwitz, B. Terheiden, R. Brendel, Staebler–Wronski-like formation of defects at the amorphous-silicon–crystalline silicon interface during illumination, J. Appl. Phys. 103 (2008) 094506.

[22] S.W. Glunz, S. Rein, J.Y. Lee, W. Warta, Minority carrier lifetime degradation in boron-doped Czochralski silicon, J. Appl. Phys. 90 (2001) 2397–2404.

[23] J. Schmidt, K. Bothe, Structure and transformation of the metastable boron- and oxygen-related defect center in crystalline silicon, Phys. Rev. B 69 (2004) 024107.

[24] J.A. del Cueto, B. von Roedern, Long-term transient and metastable effects in cadmium telluride photovoltaic modules, Prog. Photovolt. 14 (2006) 615–628.

[25] F. Engelhardt, M. Schmidt, T. Meyer, O. Seifert, J. Parisi, U. Rau, Metastable electrical transport in Cu (In, Ga) Se2 thin films and ZnO/CdS/Cu (In, Ga) Se2 heterostructures, Phys. Lett. A 245 (1998) 489–493.

[26] M. Stuckelberger, Y. Riesen, M. Despeisse, J.-W. Schüttauf, F.-J. Haug, C. Ballif, Light-induced Voc increase and decrease in high-efficiency amorphous silicon solar cells, J. Appl. Phys. 116 (2014) 094503.

[27] S. De Wolf, B. Demaurex, A. Descoeudres, C. Ballif, Very fast light-induced degradation of a-Si:H/c-Si(100) interfaces, Phys. Rev. B 83 (2011) 233301.

[28] J. Melskens, M. Schouten, A. Mannheim, A.S. Vullers, Y. Mohammadian, S.W.H. Eijt, H. Schut, T. Matsui, M. Zeman, A.H.M. Smets, The nature and the kinetics of light-induced defect creation in hydrogenated amorphous silicon films and solar cells, IEEE J. Photovolt. 4 (6) (2014) 2156–3381.

[29] R.A. Street, J. Kakalios, C.C. Tsai, T.M. Hayes, Thermal-equilibrium processes in amorphous silicon, Phys. Rev. B 35 (1987) 1316–1333.

[30] R.A. Street, M. Hack, W.B. Jackson, Mechanisms of thermal equilibration in doped amorphous silicon, Phys. Rev. B 37 (1988) 4209–4224.

[31] R.A. Street, K. Winer, Defect equilibria in undoped a-Si:H, Phys. Rev. B 40 (1989) 6236–6249.

[32] K. Winer, Chemical-equilibrium description of the gap-state distribution in a-Si:H, Phys. Rev. Lett. 63 (1989) 1487–1490.

[33] M.J. Powell, S.C. Deane, Improved defect-pool model for charged defects in amorphous silicon, Phys. Rev. B 48 (1993) 10815.

[34] M.J. Powell, S.C. Deane, Defect-pool model and the hydrogen density of states in hydrogenated amorphous silicon, Phys. Rev. B 53 (1996) 10121.

[35] G. Schumm, G.H. Bauer, Thermodynamical equilibrium gap-state distribution in undoped a-Si:H, Philos. Mag. B 64 (1991) 515–527.

[36] D.E. Carlson, C.R. Wronski, Amorphous silicon solar cell, Appl. Phys. Lett. 28 (1976) 671–673.

[37] B. Yan, G. Yue, J.M. Owens, J. Yang, S. Guha, Light-induced metastability in hydrogenated nanocrystalline silicon solar cells, Appl. Phys. Lett. 85 (2004) 1925–1927.

[38] M. Stutzmann, W.B. Jackson, C.C. Tsai, Light-induced metastable defects in hydrogenated amorphous silicon: a systematic study, Phys. Rev. B 32 (1985) 23–47.

[39] S. De Wolf, S. Olibet, C. Ballif, Stretched-exponential a-Si:H/c-Si interface recombination decay, Appl. Phys. Lett. 93 (2008) 032101.

[40] E.M. El Mhamdi, J. Holovsky, B. Demaurex, C. Ballif, S. De Wolf, Is light-induced degradation of a-Si: H/c-Si interfaces reversible? Appl. Phys. Lett. 104 (2014) 252108.

[41] A. Cuevas, R.A. Sinton, Prediction of the open-circuit voltage of solar cells from the steady-state photoconductance, Appl. Phys. Lett. 69 (1996) 2510–2512.

[42] Z.C. Holman, A. Descoeudres, L. Barraud, F.Z. Fernandez, J.P. Seif, S. De Wolf, C. Ballif, Current losses at the front of silicon heterojunction solar cells, IEEE J. Photovolt. 2 (1) (2012) 7–15.

[43] T. Söderström, P. Papet, J. Ufheil, Smart wire connection technology, in: Proceedings of the 28th European Photovoltaic Solar Energy Conference and Exhibition, Paris, France. ⟨http://dx.doi.org/10.4229/28thEUPVSEC2013-1CV.2.17⟩.

[44] M. Stutzmann, Role of mechanical stress in the light-induced degradation of hydrogenated amorphous silicon, Appl. Phys. Lett. 47 (1985) 21–23.

[45] G. Williams, D.C. Watts, Non-symmetrical dielectric relaxation behaviour arising from a simple empirical decay function, Trans. Faraday Soc. 66 (1970) 80–85.

[46] R.S. Crandall, Defect relaxation in amorphous silicon: stretched exponentials, the Meyer-Neldel rule, and the Staebler-Wronski effect, Phys. Rev. B 43 (1991) 4057–4070.

[47] J. Kakalios, R.A. Street, W.B. Jackson, Stretched-exponential relaxation arising from dispersive diffusion of hydrogen in amorphous silicon, Phys. Rev. Lett. 59 (1987) 1037–1040.

[48] A. Richter, S.W. Glunz, F. Werner, J. Schmidt, A. Cuevas, Improved quantitative description of Auger recombination in crystalline silicon, Phys. Rev. B 86 (2012) 165202.

[49] A. Descoeudres, Z.C. Holman, L. Barraud, S. Morel, S. De Wolf, C. Ballif, > 21% efficient silicon heterojunction solar cells on n-and p-type wafers compared, IEEE J. Photovolt. 3 (1) (2013) 83–89.

[50] M.J. Kerr, A. Cuevas, R.A. Sinton, Generalized analysis of quasi-steady-state and transient decay open circuit voltage measurements, J. Appl. Phys. 91 (2002) 399–404.

[51] M. Stuzmann, The defect density in amorphous silicon, Philos. Mag. B 60 (1989) 531–546.

[52] D. Redfield, R.H. Bube, Reinterpretation of degradation kinetics of amorphous silicon, Appl. Phys. Lett. 54 (1989) 1037–1039.

[53] The software package ASA of Delft University, ⟨http://pvmd.ewi.tudelft.nl/⟩.